IUST
Iran University of Science and Technology

Iranian Journal of Electrical and Electronic Engineering

Journal Homepage: ijeee.iust.ac.ir

Integrating GPS, GLONASS, BeiDou, and Galileo Receivers to Overcome Signal Blocking Challenges

K. Bahmani*, A. Sadr*, and M. R. Mosavi*(C.A.)

Abstract: Blocking interference poses significant challenges to the accuracy and reliability of navigation systems by obstructing the communication path. Single-frequency receivers are generally more susceptible to blocking interference due to their limited ability to compensate for obstructed signals or access alternative signal sources. The integration of Global Navigation Satellite Systems (GNSS) is among the most effective strategies for mitigating blocking interference. By combining signals from multiple sources, the likelihood of accessing stable and reliable signals significantly improves. The four Global GNSS include Global Positioning System (GPS), Global Navigation Satellite System (GLONASS), BeiDou, and Galileo. This paper examines the challenges of system integration in addressing navigation equations and proposes suitable solutions. Two datasets were collected under conditions of blocking disturbances, and receiver performance was simulated across 14 different modes using a software platform. The results were analyzed considering factors such as the number of satellites in view, satellite positions, extracted positions, as well as Root Mean Square (RMS), Geometric Dilution of Precision (GDOP), and Position Dilution of Precision (PDOP) parameters. In these scenarios, the GPS system in single-frequency mode, the combination of GPS and GLONASS in dual mode, and the combination of GPS, GLONASS, and Galileo in triple mode demonstrated the best performance. However, the best performance, irrespective of computational load and hardware complexity, was achieved in the quadruple integration mode.

Keywords: GPS, GLONASS, BeiDou, Galileo, Integration.

1 Introduction

THE Global Navigation Satellite System (GNSS) is a sophisticated technology designed to determine Position, Velocity, and Time (PVT) with a high degree of accuracy [1]. GNSS relies on multiple satellite constellations to provide navigation services, including the Global Positioning System (GPS) managed by the United States; the Global Navigation Satellite System (GLONASS) operated by Russia; the BeiDou Navigation Satellite System operated by China; and the Galileo system overseen by Europe [2]. Satellites in each constellation operate in various orbital configurations, such as Geostationary Orbit (GEO), medium Earth Orbit (MEO), and Inclined Geosynchronous Orbit (IGSO), sending signals to receivers on the ground to support navigation and positioning services [3,4].

As these signals travel through the Earth's atmosphere to the receivers, they can experience various changes and distortions caused by atmospheric conditions [5]. GNSS receivers are specifically designed to process this data by accurately receiving satellite signals [6]. Several key factors can influence signal quality, including the Doppler effect resulting from relative motion between the satellite and receiver, time discrepancies between satellite and receiver clocks, atmospheric delays (notably

Iranian Journal of Electrical & Electronic Engineering, 2026.
Paper first received 03 Jun 2025 and accepted 26 Aug 2025.
* The authors are with the School of Electrical Engineering, Iran University of Science and Technology (IUST), Narmak, Tehran 16846-13114, Iran.
E-mails: k_bahmani@elec.iust.ac.ir, sadr@iust.ac.ir and m_mosavi@iust.ac.ir.
Corresponding Author: M. R. Mosavi

in the troposphere and ionosphere), orbital instabilities, and signal reflections, commonly referred to as multipath interference [7,8]. Each of these factors must be carefully addressed to ensure the accuracy and reliability of GNSS systems.

Upon receiving satellite signals at the GNSS antenna, the signal processing chain is divided into four primary stages: front-end, acquisition, tracking, and navigation, as illustrated in Fig. 1 [9]. Each stage processes the signal in real time, transforming raw satellite data into valuable PVT information [10].

During the front-end stage, the signal is filtered to eliminate noise and interference, amplified to strengthen weak signals, and downconverted to an Intermediate Frequency (IF) to enable efficient processing in the subsequent stages [11]. Fig. 2 provides a detailed representation of each step in the front-end stage. Mathematically, the continuous form of the received signal from a satellite can be expressed as follows:

$$r(t) = [A.D(t-\tau).C(t-\tau).\exp(2\pi(f_c + f_d)t + \varphi)] + n(t) \quad (1)$$

where r represents the received signal, A is the signal power, D denotes the navigation data, and C is the transmitted code received by the receiver at time t. f_d represents the Doppler frequency, while τ and φ correspond to the time delays applied to the code and carrier, respectively [12]. Additionally, n represents white Gaussian noise. After sampling, the discrete form of the signal is expressed as:

$$r(mT_s) = [A.D(mT_s-\tau).C(mT_s-\tau).\exp(2\pi(f_c + f_d)mT_s + \varphi)] + n(mT_s) \quad (2)$$

where T_s is the sampling interval, and m is the number of samples per unit time. This conversion enables the signal to be processed in the digital domain [13].

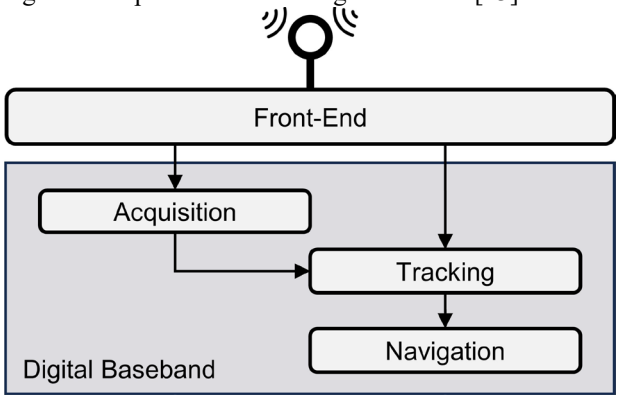

Fig 1. Block structure of GNSS receivers.

In the acquisition stage of GNSS receivers, after sampling the signals, the primary objective is to identify satellite signals and make initial estimates of essential parameters. This stage typically uses three widely applied processing methods: serial search, parallel search in the frequency domain, and parallel search in the code phase domain [14]. To enhance efficiency and accuracy during the acquisition stage, novel techniques are employed. These include Double Block Zero Padding (DBZP), which minimizes edge effects in signal processing [15], and Wavelet Transform (WT), which is highly effective for noise reduction and feature extraction [16]. Fast Fourier Transform (FFT) and its advanced variant, fractional FFT, significantly accelerate the search for Doppler shift and code phase alignment [17,18]. Post-correlation methods, including coherent integration, non-coherent integration, and differential integration, enhance the Signal-to-Noise Ratio (SNR) by combining multiple signal samples, aiding in precise parameter identification and estimation [19]. Additionally, fine acquisition methods are employed to achieve more accurate estimations, particularly in scenarios involving weak or closely spaced signals [20]. At the end of the acquisition stage, the receiver provides estimates of the Doppler frequency, code phase shift, and satellite number. These estimates are subsequently transmitted to the tracking stage for further processing [21].

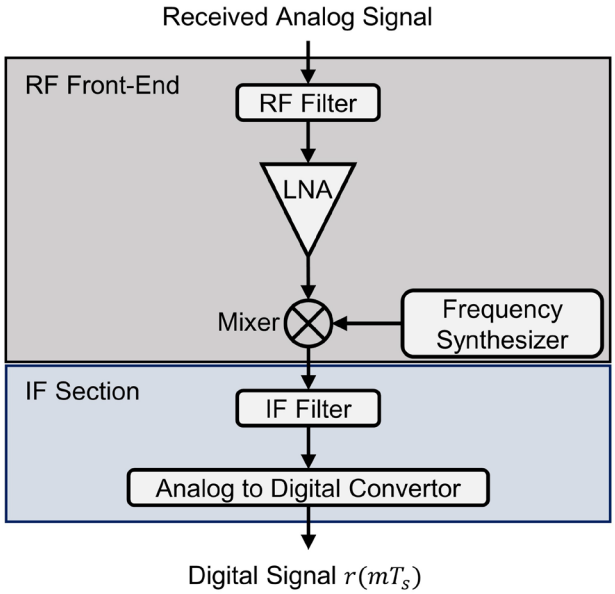

Fig 2. Block structure of the front-end stage of GNSS receivers.

In the tracking stage of GNSS receivers, the primary objective is to continuously monitor and adjust the frequency, phase, and code of each satellite signal to ensure accurate signal tracking [22]. This stage follows the acquisition stage and comprises multiple components, each responsible for specific tasks. The Phase-Locked Loop (PLL) tracker is responsible for maintaining synchronization with the phase of the received signal. By adjusting the phase of the local signal, it prevents the satellite signal from drifting. This

method is particularly effective for signals with a high Carrier-to-Noise Ratio (CNR) [23]. The Delay-Locked Loop (DLL) tracker monitors changes in the signal code over time and adjusts the timing to align the local signal with the received one. This process ensures precise tracking of the code location and maintains signal synchronization [24]. The Frequency-Locked Loop (FLL) detector aligns the frequency of the received signal with the local frequency. It is particularly effective for signals with higher relative motion, where frequency variations are more pronounced [25]. In addition to these standard tracking loops, modern approaches such as neural network-based techniques and machine learning are employed to enhance tracking accuracy, especially in noisy or weak signal environments [26]. Moreover, the integration of PLL and FLL techniques is employed to enhance both accuracy and stability, particularly in challenging and operating environments [27]. Upon completing the tracking stage at each time interval, the output provides accurate information on the frequency, phase, and code errors of each signal. These errors are used in the next phase of tracking to maintain signal alignment and validate navigation data for accurate position determination [28].

In the navigation stage, the GNSS receiver extracts navigation bits that contain essential information for determining position [29]. As shown in Fig. 3, the first step in processing these bits is bit edge detection [30]. This step is crucial as it allows the receiver to identify the boundaries of each bit accurately, preventing temporal interference and minimizing errors in data interpretation [31]. After that, the receiver looks for preamble bits. These preamble bits mark the start of a new data frame and help the receiver correctly recognize the structure and sequence of the received frames [32]. Then, the receiver enters the frame and subframe recognition phase. These frames have distinct structures for each constellation [33]. For example, in GPS, each frame is divided into five subframes that contain critical information, such as the time of transmission used to calculate time delay and satellite distance, precise orbital parameters referred to as Ephemeris that provide short-term orbital details of each satellite, and general constellation data referred to as almanac that offers long-term approximate orbital information for all satellites in the constellation [34]. It also includes time and atmospheric error correction information that enables the receiver to compensate for atmospheric effects during its calculations. The frame structure in GLONASS, BeiDou, and Galileo differs as well and is specifically designed to meet the unique requirements of each system and the type of data they provide [35]. Using this data, the receiver can determine the position of each satellite in the sky at a specific time [36]. There are several methods for determining a satellite's position, including constant geocentric coordinates, known as Earth-Centered Earth-Fixed (ECEF) coordinates, which provide the three-dimensional position of the satellite relative to the Earth's center. Using these coordinates along with precise time data, the receiver can calculate the distance to each satellite and, ultimately, its own position [37].

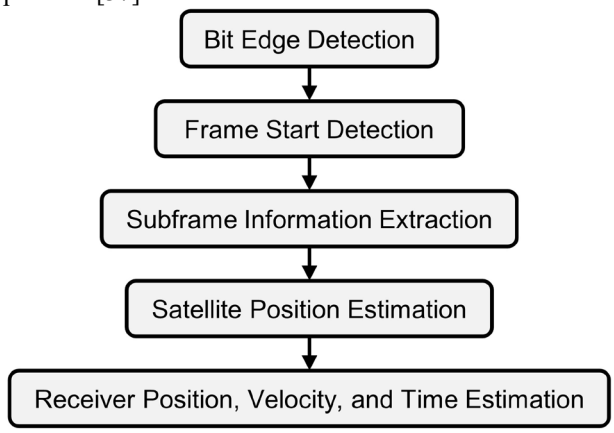

Fig 3. Navigation information processing steps for determining receiver PVT.

As shown in Fig. 4, blocking in GNSS signals refers to the disruption or attenuation of satellite signals, which can significantly affect the performance of GNSS receivers. This phenomenon is caused by various factors, including physical obstacles such as tall buildings or hills that block the Line of Sight (LOS) between the satellites and the receiver, Electromagnetic Interference (EMI) from devices operating on similar frequencies, and adverse weather conditions, such as heavy rain or thunderstorms, which can weaken signals as they propagate through the atmosphere [38]. Consequences of blocking include loss of lock, where the receiver can no longer track satellite signals, increased error rates that result in inaccurate position estimates, and delays in real-time estimates, which can negatively impact applications that depend on real-time GNSS data [39].

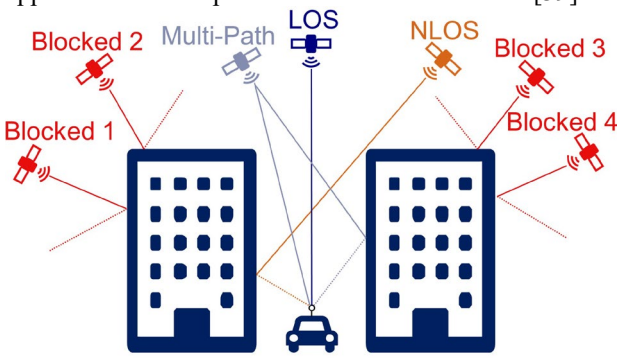

Fig 4. Illustration of signal blocking in GNSS systems.

Single-frequency GNSS systems face considerable

accuracy challenges in environments such as dense urban areas, forests, or mountainous regions. These obstructions can cause multipath errors, limit satellite visibility, and reduce positioning accuracy due to signal instability in such conditions [40]. To address these limitations, various methods have been developed to enhance GNSS accuracy. A common approach involves combining single-frequency GNSS systems with additional sensors, such as Inertial Navigation Systems (INS) or Inertial Measurement Units (IMUs), which help maintain position estimates even when satellite signals are weak or unavailable [41]. By integrating GNSS with these sensors, positioning accuracy is significantly enhanced, particularly during short periods of GNSS signal loss. However, this approach requires the receiver to incorporate additional hardware and equipment associated with these sensors [42].

Another class of techniques for improving positioning accuracy is Differential GNSS (DGNSS), where a network of reference stations transmits corrections to the GNSS receiver in real time. These corrections help reduce positioning errors caused by atmospheric delays and satellite-related factors. This method significantly enhances positioning accuracy, particularly at short to medium ranges, and is widely used in various precision applications [43,44]. The third class involves the use of Space-Based Augmentation Systems (SBAS) and Ground-Based Augmentation Systems (GBAS). SBAS provides corrections over a wide area by transmitting correction data from satellites, improving accuracy by compensating for atmospheric and other errors on a regional scale [45]. Conversely, GBAS operates over shorter distances, typically near airports, to deliver precise corrections that are especially beneficial for aircraft navigation. However, the second and third categories are not feasible in all areas and depend on the presence of reference stations within the LOS of the receiver [46].

Another class involves combining multiple GNSS systems, such as GPS with GLONASS or GPS with BeiDou, to enhance positioning reliability in obstructed environments by increasing the number of available satellites [47,48]. This method is particularly beneficial for applications that demand high accuracy in challenging conditions, as integrated systems provide additional satellite options and reduce dependence on any single GNSS. In recent research, this multi-system combination has been applied in Precise Point Positioning (PPP) and Real-Time Kinematics (RTK) methods [49]. PPP utilizes precise satellite orbit and clock data to achieve centimeter-level accuracy on a global scale without requiring a base station, while RTK offers high accuracy over short distances by employing carrier phase measurements and corrections from a nearby base station [50]. In these studies, researchers frequently use Receiver Independent Exchange Format (RINEX) files to standardize and process GNSS data for accuracy assessment.

In our proposed method, we address the challenges of positioning in environments with severe signal obstruction by integrating signals from four GNSS constellations: GPS, GLONASS, BeiDou, and Galileo. Relying on a single GNSS system in such conditions often proves insufficient due to limited satellite visibility. To overcome this, we use real data collected by a high-bandwidth GNSS front-end receiver capable of simultaneously capturing signals from all four systems. The raw signals are digitized, and acquisition is performed separately for each constellation. Subsequently, tracking is conducted for each satellite in view. The tracking results are then forwarded to the navigation solution stage, where multi-constellation observations are fused to estimate the receiver's position. This approach enhances positioning accuracy, particularly in challenging environments.

In the following sections, the proposed method is described in detail, including the process of integrating observation vectors from multiple navigation systems to enhance positioning accuracy. Subsequently, the procedure for real data collection is outlined, along with descriptions of the hardware and software used in the experimental setup. The evaluation criteria, namely Dilution of Precision (DOP) and Root Mean Square (RMS), are then introduced, along with the relevant equations and computational methods used to assess system performance. Finally, simulation results from two different scenarios are presented and analyzed to provide a comprehensive assessment of the performance of the proposed method under varying conditions. The paper concludes by summarizing the key findings and contributions of the research.

2 Proposed Method

Once the satellite position has been determined, the next step is to calculate the receiver's position. This is achieved by utilizing the pseudo-range or carrier phase observation equations [51,52], which provide the measured distance between the receiver and the satellite. In the case of pseudo-range, the distance is determined by measuring the signal's travel time from the satellite to the receiver and converting it into distance units by multiplying it by the signal propagation speed (the speed of light). For the carrier phase, the apparent distance is derived by counting the number of carrier cycles during the signal's transmission and multiplying this count by the signal's wavelength. The equations for both methods are presented below:

$$P_r^s = c.t_r^s = \rho_r^s + c(dt_r - dt^s) + T_r^s + I_r^s + e_r^s \qquad (3)$$

$$\Phi_r^s = \lambda\varphi_r^s = \rho_r^s + c(dt_r - dt^s) + T_r^s - I_r^s + \lambda N + e_r^s \quad (4)$$

Here, P and Φ denote the apparent distances obtained from the pseudo-range and carrier phase methods, respectively. The indices r and s represent the receiver and the satellite, respectively. c and λ refer to the speed of light in a vacuum ($299{,}792{,}458\,m/s$) and the signal wavelength, respectively. t is the signal arrival time, φ is the number of carrier cycles, ρ is the geometric distance, dt is the receiver clock offset (in seconds), T represents the tropospheric delay, I accounts for the ionospheric delay, and N is the carrier phase ambiguity integer. Additionally, e captures other error sources, such as multipath effects and satellite orbit inaccuracies.

The carrier frequencies of GNSS signals are more than 1,000 times higher than the frequencies of the measurement codes. This significant difference enables the carrier phase measurement method to achieve apparent distance estimations with an accuracy up to three orders of magnitude higher than that of pseudo-range measurements. However, due to the uniformity of the carrier phase, the exact number of cycles cannot be determined, resulting in an integer ambiguity in the carrier phase cycles [53]. Consequently, the pseudo-range equations are utilized for further calculations. The geometric distance between the satellite and the receiver is determined using the following relationship:

$$\rho_r^s = \sqrt{(X^s - X_r)^2 + (Y^s - Y_r)^2 + (Z^s - Z_r)^2} \quad (5)$$

Here, (X, Y, Z) represents the geometric coordinates of the satellite and receiver positions. By substituting Eq. (5) into Eq. (3), we obtain:

$$c.t_r^s = \sqrt{(X^s - X_r)^2 + (Y^s - Y_r)^2 + (Z^s - Z_r)^2} + c(dt_r - dt^s) + T_r^s + I_r^s + e_r^s \quad (6)$$

The equation above is nonlinear with respect to the receiver's position [54]. To linearize it, the receiver's position is treated as a variable:

$$f(X_r, Y_r, Z_r) = \sqrt{(X^s - X_r)^2 + (Y^s - Y_r)^2 + (Z^s - Z_r)^2} \quad (7)$$

The receiver's position at time t is expressed as:

$$X_r(t) = X_r(t-1) + \Delta X_r \quad (8)$$

$$Y_r(t) = Y_r(t-1) + \Delta Y_r \quad (9)$$

$$Z_r(t) = Z_r(t-1) + \Delta Z_r \quad (10)$$

By substituting Eq.s (8) to (10) into Eq. (7) and applying the Taylor series expansion under the assumption that higher-order terms are negligible, we obtain Eq (11). At the initial moment, the value of $f\big(X_r(t-1), Y_r(t-1), Z_r(t-1)\big)$ is given by Eq (12). By substituting Eq. (12) into Eq. (11), we obtain the expression for the first moment given in Eq. (13). We insert the solution of Eq. (13) into Eq. (3), yielding Eq (14). By rearranging the equation to place the known values on one side and the unknowns on the other, we obtain Eq(15).

$$f(X_r(t), Y_r(t), Z_r(t)) = f\big(X_r(t-1), Y_r(t-1), Z_r(t-1)\big) - \frac{[X^s - X_r(t-1)]\Delta X_r + [Y^s - Y_r(t-1)]\Delta Y_r + [Z^s - Z_r(t-1)]\Delta Z_r}{f\big(X_r(t-1), Y_r(t-1), Z_r(t-1)\big)} \quad (11)$$

$$\rho_r^s(0) = \sqrt{(X^s - X_r(0))^2 + (Y^s - Y_r(0))^2 + (Z^s - Z_r(0))^2} \quad (12)$$

$$\rho_r^s(1) = \rho_r^s(0) - \frac{X^s - X_r(0)}{\rho_r^s(0)}\Delta X_r - \frac{Y^s - Y_r(0)}{\rho_r^s(0)}\Delta Y_r - \frac{Z^s - Z_r(0)}{\rho_r^s(0)}\Delta Z_r \quad (13)$$

$$P_r^s = \rho_r^s(0) - \frac{X^s - X_r(0)}{\rho_r^s(0)}\Delta X_r - \frac{Y^s - Y_r(0)}{\rho_r^s(0)}\Delta Y_r - \frac{Z^s - Z_r(0)}{\rho_r^s(0)}\Delta Z_r + c(dt_r - dt^s) + T_r^s + I_r^s + e_r^s \quad (14)$$

$$-\frac{X^s - X_r(0)}{\rho_r^s(0)}\Delta X_r - \frac{Y^s - Y_r(0)}{\rho_r^s(0)}\Delta Y_r - \frac{Z^s - Z_r(0)}{\rho_r^s(0)}\Delta Z_r + c.dt_r = P_r^s - \rho_r^s(0) + c.dt^s - T_r^s - I_r^s - e_r^s \quad (15)$$

The above equation contains four unknowns, meaning at least four equations are required to solve it. When the number of equations is equal to or greater than the number of unknowns, the Least Squares (LS) error method can be applied. To proceed, we first express Eq. (15) in matrix form:

$$\begin{bmatrix} -\frac{X^s - X_r(0)}{\rho_r^s(0)} & -\frac{Y^s - Y_r(0)}{\rho_r^s(0)} & -\frac{Z^s - Z_r(0)}{\rho_r^s(0)} & c \end{bmatrix} \begin{bmatrix} \Delta X_r \\ \Delta Y_r \\ \Delta Z_r \\ dt_r \end{bmatrix} = k \quad (16)$$

Here, k is defined as $P_r^s - \rho_r^s(0) + c.dt^s - T_r^s - I_r^s - e_r^s$. The observation equation for a single GNSS system is constructed using n visible satellites, where each row of the design matrix corresponds to the unit LOS vector from the receiver to a satellite. The associated unknown vector consists of the receiver's position corrections along with a single clock bias term. The linearized observation equation is expressed as follows:

$$\begin{bmatrix} -\frac{X^{s,1} - X_r(0)}{\rho_r^{s,1}(0)} & -\frac{Y^{s,1} - Y_r(0)}{\rho_r^{s,1}(0)} & -\frac{Z^{s,1} - Z_r(0)}{\rho_r^{s,1}(0)} & c \\ -\frac{X^{s,2} - X_r(0)}{\rho_r^{s,2}(0)} & -\frac{Y^{s,2} - Y_r(0)}{\rho_r^{s,2}(0)} & -\frac{Z^{s,2} - Z_r(0)}{\rho_r^{s,2}(0)} & c \\ \vdots & \vdots & \vdots & \vdots \\ -\frac{X^{s,n} - X_r(0)}{\rho_r^{s,n}(0)} & -\frac{Y^{s,n} - Y_r(0)}{\rho_r^{s,n}(0)} & -\frac{Z^{s,n} - Z_r(0)}{\rho_r^{s,n}(0)} & c \end{bmatrix} \begin{bmatrix} \Delta X_r \\ \Delta Y_r \\ \Delta Z_r \\ dt_r \end{bmatrix} = K \quad (17)$$

When multiple GNSS constellations are combined in a

single navigation solution, the observation model must be extended to account for constellation-specific clock biases. Since each GNSS system maintains its own time reference, a distinct receiver clock offset must be estimated for each system, in addition to the common position corrections. As a result, the observation matrix expands: the number of rows increases with the total number of visible satellites across all constellations, and the number of columns grows to include one clock bias term per system. This ensures that all pseudorange measurements are correctly aligned with their respective system times and enables consistent integration across GPS, GLONASS, BeiDou, and Galileo. Under these conditions, the single-system observation equation presented in Eq. (17) is generalized and rewritten as shown in Eq. (18), reflecting the combined multi-GNSS model.

$$\begin{bmatrix}
-\frac{X_{GPS}^{s,1}-X_r(0)}{\rho_{r,GPS}^{s,1}(0)} & -\frac{Y_{GPS}^{s,1}-Y_r(0)}{\rho_{r,GPS}^{s,1}(0)} & -\frac{Z_{GPS}^{s,1}-Z_r(0)}{\rho_{r,GPS}^{s,1}(0)} & c & 0 & 0 & 0 \\
-\frac{X_{GPS}^{s,2}-X_r(0)}{\rho_{r,GPS}^{s,2}(0)} & -\frac{Y_{GPS}^{s,2}-Y_r(0)}{\rho_{r,GPS}^{s,2}(0)} & -\frac{Z_{GPS}^{s,2}-Z_r(0)}{\rho_{r,GPS}^{s,2}(0)} & c & 0 & 0 & 0 \\
\vdots & \vdots & \vdots & \vdots & \vdots & \vdots & \vdots \\
-\frac{X_{GPS}^{s,n}-X_r(0)}{\rho_{r,GPS}^{s,n}(0)} & -\frac{Y_{GPS}^{s,n}-Y_r(0)}{\rho_{r,GPS}^{s,n}(0)} & -\frac{Z_{GPS}^{s,n}-Z_r(0)}{\rho_{r,GPS}^{s,n}(0)} & c & 0 & 0 & 0 \\
-\frac{X_{GLO}^{s,1}-X_r(0)}{\rho_{r,GLO}^{s,1}(0)} & -\frac{Y_{GLO}^{s,1}-Y_r(0)}{\rho_{r,GLO}^{s,1}(0)} & -\frac{Z_{GLO}^{s,1}-Z_r(0)}{\rho_{r,GLO}^{s,1}(0)} & 0 & c & 0 & 0 \\
-\frac{X_{GLO}^{s,2}-X_r(0)}{\rho_{r,GLO}^{s,2}(0)} & -\frac{Y_{GLO}^{s,2}-Y_r(0)}{\rho_{r,GLO}^{s,2}(0)} & -\frac{Z_{GLO}^{s,2}-Z_r(0)}{\rho_{r,GLO}^{s,2}(0)} & 0 & c & 0 & 0 \\
\vdots & \vdots & \vdots & \vdots & \vdots & \vdots & \vdots \\
-\frac{X_{GLO}^{s,m}-X_r(0)}{\rho_{r,GLO}^{s,m}(0)} & -\frac{Y_{GLO}^{s,m}-Y_r(0)}{\rho_{r,GLO}^{s,m}(0)} & -\frac{Z_{GLO}^{s,m}-Z_r(0)}{\rho_{r,GLO}^{s,m}(0)} & 0 & c & 0 & 0 \\
-\frac{X_{BDS}^{s,1}-X_r(0)}{\rho_{r,BDS}^{s,1}(0)} & -\frac{Y_{BDS}^{s,1}-Y_r(0)}{\rho_{r,BDS}^{s,1}(0)} & -\frac{Z_{BDS}^{s,1}-Z_r(0)}{\rho_{r,BDS}^{s,1}(0)} & 0 & 0 & c & 0 \\
-\frac{X_{BDS}^{s,2}-X_r(0)}{\rho_{r,BDS}^{s,2}(0)} & -\frac{Y_{BDS}^{s,2}-Y_r(0)}{\rho_{r,BDS}^{s,2}(0)} & -\frac{Z_{BDS}^{s,2}-Z_r(0)}{\rho_{r,BDS}^{s,2}(0)} & 0 & 0 & c & 0 \\
\vdots & \vdots & \vdots & \vdots & \vdots & \vdots & \vdots \\
-\frac{X_{BDS}^{s,p}-X_r(0)}{\rho_{r,BDS}^{s,p}(0)} & -\frac{Y_{BDS}^{s,p}-Y_r(0)}{\rho_{r,BDS}^{s,p}(0)} & -\frac{Z_{BDS}^{s,p}-Z_r(0)}{\rho_{r,BDS}^{s,p}(0)} & 0 & 0 & c & 0 \\
-\frac{X_{GAL}^{s,1}-X_r(0)}{\rho_{r,GAL}^{s,1}(0)} & -\frac{Y_{GAL}^{s,1}-Y_r(0)}{\rho_{r,GAL}^{s,1}(0)} & -\frac{Z_{GAL}^{s,1}-Z_r(0)}{\rho_{r,GAL}^{s,1}(0)} & 0 & 0 & 0 & c \\
-\frac{X_{GAL}^{s,2}-X_r(0)}{\rho_{r,GAL}^{s,2}(0)} & -\frac{Y_{GAL}^{s,2}-Y_r(0)}{\rho_{r,GAL}^{s,2}(0)} & -\frac{Z_{GAL}^{s,2}-Z_r(0)}{\rho_{r,GAL}^{s,2}(0)} & 0 & 0 & 0 & c \\
\vdots & \vdots & \vdots & \vdots & \vdots & \vdots & \vdots \\
-\frac{X_{GAL}^{s,q}-X_r(0)}{\rho_{r,GAL}^{s,q}(0)} & -\frac{Y_{GAL}^{s,q}-Y_r(0)}{\rho_{r,GAL}^{s,q}(0)} & -\frac{Z_{GAL}^{s,q}-Z_r(0)}{\rho_{r,GAL}^{s,q}(0)} & 0 & 0 & 0 & c
\end{bmatrix}
\begin{bmatrix} \Delta X_r \\ \Delta Y_r \\ \Delta Z_r \\ dt_r^{GPS} \\ dt_r^{GLO} \\ dt_r^{BDS} \\ dt_r^{GAL} \end{bmatrix} = K \tag{18}$$

In the above equation, GPS, GLO, BDS, and GAL represent the GPS, GLONASS, BeiDou, and Galileo systems, respectively. With seven unknowns in this equation, combining four systems requires at least seven equations to solve. The dimensions of the observation matrix are $(m+n+p+q)\times 7$, and the unknowns are represented by a 7×1 vector. If we denote the vector of observations by H and the best estimate of the unknowns, which minimizes the LS error, by $\hat{x}$, we have:

$$H.\hat{x} = K \tag{19}$$

Consequently, the unknowns can be determined as follows:

$$H^T H.\hat{x} = H^T K \rightarrow \hat{x} = (H^T H)^{-1} H^T K \tag{20}$$

The purpose of GNSS signal integration is to enhance the reliability and accuracy of the navigation receiver, particularly in the presence of disturbances such as signal blockage. This integration increases the number of LOS satellites, ensuring that even if the number of LOS satellites in a single GNSS system falls below four, the receiver can still perform accurate positioning. With this proposed method, in addition to enhancing reliability, positioning accuracy is also improved, as the combined data from multiple GNSS systems enables error compensation and provides more precise position information.

To clearly illustrate the multi-GNSS integration process, Fig. 5 presents a step-by-step pseudocode of the implemented signal processing framework. The procedure begins with independent signal acquisition for

each visible constellation using raw IF data. Following acquisition, each satellite is tracked in real time through standard code and carrier tracking loops. The integration stage evaluates all 14 possible combinations of GNSS constellations. For each configuration, the visible satellites are selected, and a corresponding observation matrix is constructed. Finally, the navigation equations are solved using a LS approach to determine the position solution.

```
Input: Raw IF signal (L1C, GL1, B1I, E1C)

for each GNSS constellation do
   → Perform acquisition
   → Estimate code phase, Doppler, carrier phase
end for

for each satellite in view do
   → Track using code & carrier loops
end for

for each integration mode do
   → Select visible, tracked satellites
   → Build observation matrix
   → Apply LS to solve navigation equations
end for

Output: Position solutions for all integration modes
```

Fig 5. Pseudocode of the multi-GNSS signal processing and integration procedure.

3 Dataset and Experimental Setup

In this study, two datasets were collected under signal-blocking conditions at Iran University of Science and Technology (IUST), specifically around the university's electrical laboratory. The first dataset was recorded near the entrance door of the laboratory. This area is obstructed on the southern side by the building, and the presence of trees in the vicinity further disrupts the reception of navigation signals. The second dataset was gathered near a window on the second floor of the laboratory building. This location is obstructed on the northern side by the building, allowing signal transmission only through the window, with limited satellite visibility for the receiver. These environments were deliberately chosen to replicate real-world GNSS signal degradation caused by urban infrastructure and natural obstructions. In both scenarios, no artificial satellite blocking was introduced; instead, the receiver was passively exposed to realistic signal loss conditions. The datasets provide valuable insight into how multi-GNSS integration performs when each individual constellation alone is insufficient for standalone positioning.

Table 1 presents the positions of the two datasets, including their longitude, latitude, and altitude, recorded on a specific date and time. This location data is utilized to analyze the blocking conditions and their impact on the quality of signals received from navigation systems.

In this study, raw GNSS signals were collected using a high-bandwidth front-end receiver capable of simultaneously capturing L1C (GPS), GL1 (GLONASS), B1I (BeiDou), and E1C (Galileo) signals at a high sampling rate. After digitization, the signals were processed through independent acquisition modules for each constellation to estimate code phase and Doppler frequency. Tracking was then performed for all visible satellites. This configuration enabled a unified receiver structure in which tracking results could be reliably fused in the navigation solution. A system equipped with an Intel Core i7-6500U processor and 16 GB of RAM was employed for simulations, while MATLAB 2021b software was used for data analysis and computations in the navigation stage. The LOS satellites for the GPS, GLONASS, BeiDou, and Galileo navigation systems, as derived from the acquisition stage for the first and second datasets, are illustrated in Figures 6 and 7. As shown, the number of LOS satellites in both datasets is limited. This limited satellite visibility directly affects positioning performance: for the first dataset, single-frequency receivers face significant challenges, while for the second dataset, positioning is infeasible due to having fewer than four visible satellites. Here, the objective is to integrate the visible satellites across constellations to enable accurate and reliable positioning.

Table 1. Position parameters, and timestamp for the first and second datasets.

Parameter	Dataset Value	
	1	2
Date (ISO 8601)	2024-10-27	2024-10-27
Time (UTC)	7:10:30	8:35:33
Longitude (°E)	51.506282	51.506263
Latitude (°N)	35.743101	35.742812
Altitude (m)	1319.3	1323.1

4 GNSS Benchmarks

In GNSS, positioning accuracy is measured using criteria known as DOP parameters, or accuracy reduction factors. Two significant parameters are Geometric Dilution of Precision (GDOP) and Position Dilution of Precision (PDOP), both of which affect the accuracy and calculation errors in position determination [55]. These parameters are calculated based on the geometry and the angles between the satellites and the receiver, representing how the satellites are dispersed in the sky relative to the receiver. Generally, a lower DOP

value indicates higher positioning accuracy. It should be noted that a wider distribution of satellites in the sky results in a lower DOP value, while a closer positioning of satellites increases the DOP value. The Q matrix is defined as the covariance matrix of the observation matrix, as follows:

$$Q = (H^T H)^{-1} = \begin{bmatrix} q_{x^2} & q_{xy} & q_{xz} & q_{xt} \\ q_{xy} & q_{y^2} & q_{yz} & q_{yt} \\ q_{xz} & q_{yz} & q_{z^2} & q_{zt} \\ q_{xt} & q_{yt} & q_{zt} & q_{t^2} \end{bmatrix} \quad (21)$$

The value of DOP can be extracted in the following way:

$$DOP = \sqrt{trace(Q)} \quad (22)$$

The accuracy of the three-dimensional position, including latitude, longitude, and altitude, is evaluated by the PDOP parameter and is defined as follows:

$$PDOP = \sqrt{q_{x^2} + q_{y^2} + q_{z^2}} \quad (23)$$

In GDOP, time changes, along with position changes, are also involved and are represented as follows:

$$GDOP = \sqrt{q_{x^2} + q_{y^2} + q_{z^2} + q_{t^2}} \quad (24)$$

Deviation from the RMS criterion is a statistical measure used to assess the dispersion of data relative to their average value [56,57]. The smaller RMS value, the closer the data aligns with the mean value. In this case, instead of using the average spatial coordinates, we consider the exact location of the receiver in static mode and define RMS as follows:

$$RMS = \sqrt{\frac{1}{B}\sum_{b=1}^{B}\left[\left(X_{r,b} - X_{r,true}\right)^2 + \left(Y_{r,b} - Y_{r,true}\right)^2 + \left(Z_{r,b} - Z_{r,true}\right)^2\right]} \quad (25)$$

Where B is the number of calculation repetitions, $(X_{r,true}, Y_{r,true}, Z_{r,true})$ represents the true position of the receiver, and $(X_{r,b}, Y_{r,b}, Z_{r,b})$ denotes the estimated position in iteration b. In this paper, these criteria are used to evaluate the performance and accuracy of single-frequency receivers and integrated receivers.

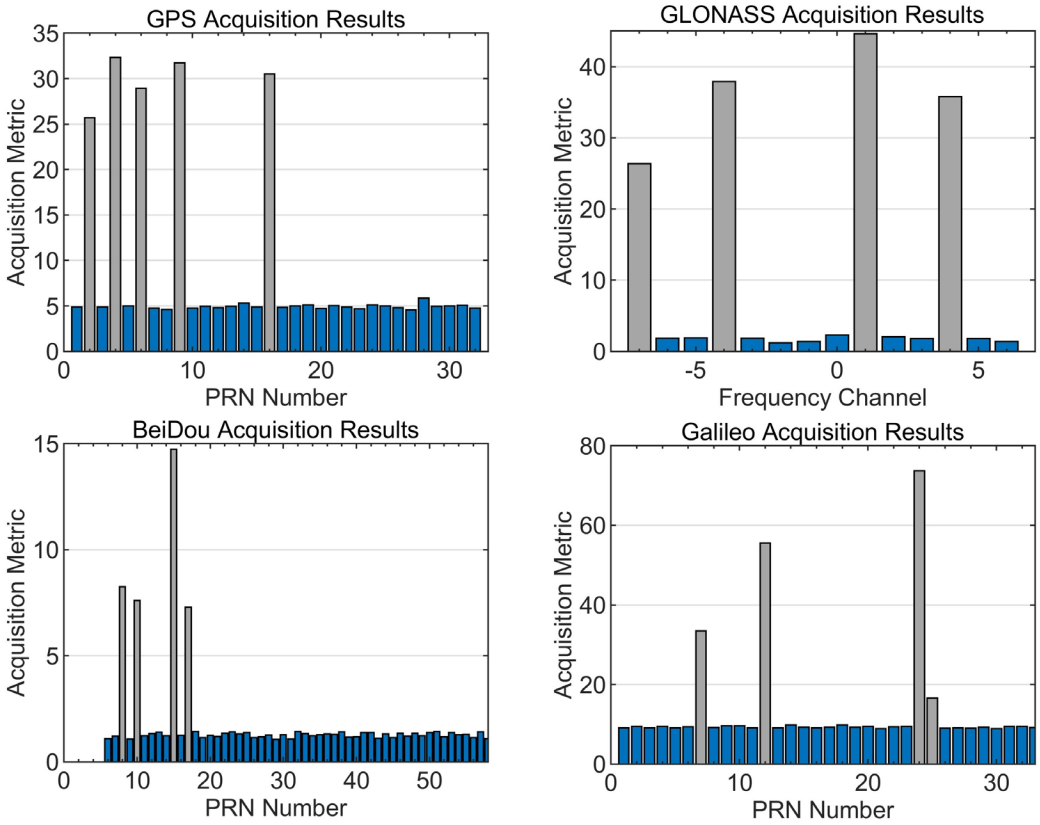

Fig 6. LOS satellites identified during the acquisition stage for the first dataset.

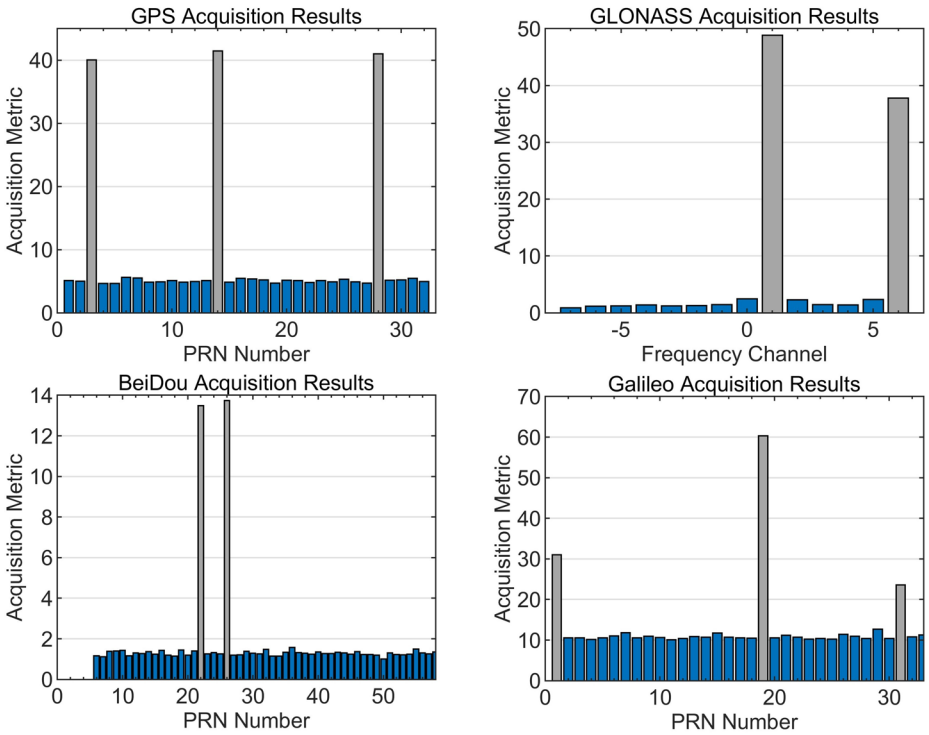

Fig 7. LOS satellites identified during the acquisition stage for the second dataset.

5 Results

This section provides a detailed analysis of both standalone and integrated navigation systems from various perspectives, including satellite positioning, RMS error, and the GDOP and PDOP criteria. By examining these factors, the performance and accuracy of different navigation systems are compared, revealing how each system performs under specific scenarios. Based on the results, the most suitable system will be identified according to the outlined criteria and recommended as the optimal choice for navigation applications.

The satellite positions relative to the receiver in two different datasets have been examined. Fig. 8 shows the satellite positions for the first dataset, while Fig. 9 shows the satellite positions for the second dataset. As illustrated in Fig. 8, the number of satellites in the first dataset is greater than four for single-frequency receivers, enabling single-frequency tracking. In contrast, the number of satellites in the second dataset is fewer than four, preventing the receiver from performing single-frequency tracking. The LOS angles of the satellites in the first dataset are more favorable and optimized. However, in the second dataset, due to data collection in an enclosed space, only satellites with lower horizon angles are visible to the receiver. In this case, considering the existing conditions, the integration of systems during the positioning process is essential to obtain accurate positioning and improve precision.

Using the collected data, the signal acquisition, tracking, and navigation equation-solving processes were carried out with high accuracy. The average geographic coordinates, including longitude, latitude, and altitude, estimated in both the integrated and standalone modes, are presented in Table 2. For the first dataset, the GPS system provided the closest estimate to the actual position, while the GLONASS system exhibited the lowest positioning accuracy. In the second dataset, none of the single-frequency systems were able to determine the receiver's position. However, the four-system integrated receiver achieved the highest accuracy and provided significant results. It is worth noting that due to the insufficient number of satellites from the GLONASS and BeiDou systems, positioning in the integrated mode of these two systems was not possible.

For a more accurate evaluation, RMS values were calculated using Eq. (25), and the results are shown in Fig. 10. The RMS value was calculated for the first 65 seconds. Analysis of the results indicates that, in the two scenarios examined, the single-frequency receivers in the first dataset performed differently, with the GPS system providing the best accuracy and the GLONASS system providing the lowest. However, in the second dataset, none of the single-frequency receivers were able to perform independent positioning. In the dual integration mode, for the first dataset, the best accuracy was achieved by integrating GPS and Galileo, while for the second dataset, the combination of GPS and

GLONASS performed better. On the other hand, the lowest accuracy in the first dataset was observed with the integration of BeiDou and Galileo. In the second dataset, the combination of GLONASS and BeiDou was unable to perform accurate positioning. In the triple integration mode, the best accuracy in both datasets was obtained by combining GPS, GLONASS, and Galileo. However, the lowest accuracy in the first dataset was associated with the combination of GLONASS, BeiDou, and Galileo, and in the second dataset, it was linked to the combination of GPS, GLONASS, and BeiDou. These results demonstrate that the choice of an appropriate system combination has a significant impact on positioning accuracy and reliability, especially in conditions where single-frequency systems perform poorly.

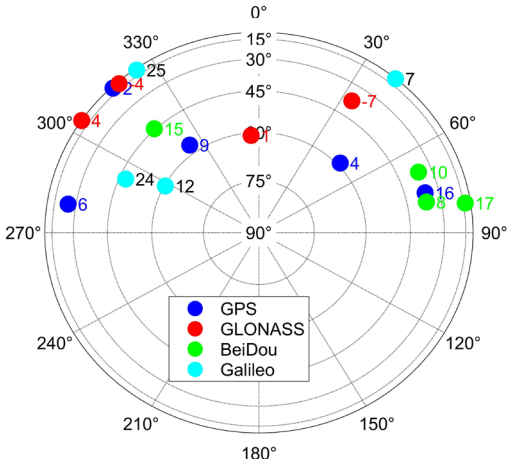

Fig 8. Satellite positions relative to the receiver for the first dataset.

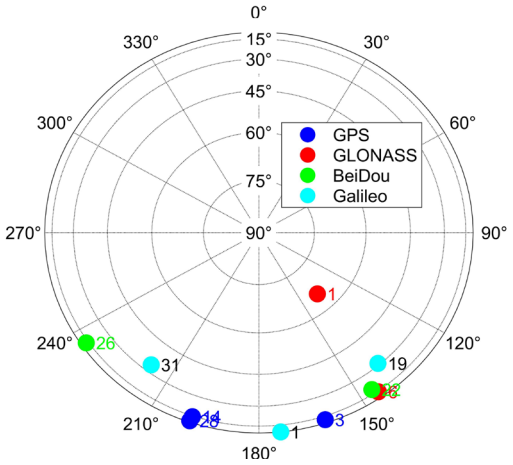

Fig 9. Satellite positions relative to the receiver for the second dataset.

The GDOP and PDOP results in different modes for the first and second datasets are shown in Fig. 11. The behavior of GDOP and PDOP in both datasets is nearly identical. In both scenarios, the four-system integrated receiver yielded the most accurate results. The analysis of the results indicates that integration generally improves the DOP values and enhances positioning accuracy.

Table 2. Average estimated longitude, latitude, and altitude in different modes for the first and second datasets.

Mode	Latitude (°N)		Longitude (°E)		Altitude (m)	
	Dataset1	Dataset2	Dataset1	Dataset2	Dataset1	Dataset2
GPS	35°44/35.1606	-	51°30/22.6741	-	1301.2	-
GLO	35°44/28.3650	-	51°30/25.0166	-	1193.1	-
BDS	35°44/29.3292	-	51°30/18.6058	-	1348.3	-
GAL	35°44/34.5681	-	51°30/23.3689	-	1291.4	-
GPS+GLO	35°44/34.7687	35°44/38.2548	51°30/22.8358	51°30/24.2975	1289.9	1222.5
GPS+BDS	35°44/36.1892	35°44/58.7195	51°30/21.6698	51°30/24.4743	1355.6	1122.0
GPS+GAL	35°44/35.0938	35°44/24.1840	51°30/22.9119	51°30/22.6890	1293.6	1404.3
GLO+BDS	35°44/36.5903	-	51°30/21.2279	-	1348.8	-
GLO+GAL	35°44/32.5374	35°45/8.0460	51°30/23.5973	51°30/20.2652	1252.0	504.3
BDS+GAL	35°44/39.3061	35°44/42.2462	51°30/22.5429	51°30/21.3030	1383.2	1033.5
GPS+GLO+BDS	35°44/36.1513	35°44/51.6646	51°30/21.7522	51°30/23.8962	1341.6	921.1
GPS+GLO+GAL	35°44/34.6674	35°44/44.0096	51°30/22.9833	51°30/22.0080	1285.0	1009.5
GLO+BDS+GAL	35°44/37.8332	35°44/43.1812	51°30/22.0042	51°30/21.3498	1338.5	1051.3
GPS+GLO+BDS+GAL	35°44/36.8399	35°44/44.8769	51°30/22.2048	51°30/22.0489	1329.7	1318.9

To statistically validate the improvements achieved through multi-GNSS integration, two-sample t-tests were conducted between the standalone GPS configuration and each integration mode that includes

GPS, using a dataset collected under signal-blocking conditions. The dataset comprises 700 samples recorded every 100 ms over a 70-second period. At each epoch, the RMS of positioning errors, GDOP, and PDOP were computed for each configuration. Table 3 reports the resulting p-values, where values below 0.05 indicate statistically significant improvements over standalone GPS. The GPS+GLO+BDS+GAL combination achieved highly significant results across all metrics, confirming substantial gains in both positioning accuracy and satellite geometry. Similarly, GPS+GLO+GAL showed a strong improvement in RMS, and GPS+GLO+BDS achieved significant gains across all metrics. These results highlight the effectiveness of integrating multiple GNSS constellations, particularly when three or more are combined.

Table 3. P-values comparing GPS with GPS-based integrations in Dataset 1 for RMS, GDOP, and PDOP.

Mode	p-value		
	RMS	GDOP	PDOP
GPS+GLO	2.1e-132	2.3e-02	3.9e-02
GPS+BDS	1.6e-120	1.9e-01	6.2e-01
GPS+GAL	6.3e-173	8.2e-01	2.9e-01
GPS+GLO+BDS	2.8e-134	2.6e-02	1.6e-02
GPS+GLO+GAL	1.7e-158	6.1e-02	1.4e-01
GPS+GLO+BDS+GAL	3.2e-147	3.3e-04	2.8e-06

In general, Table 4 categorizes the various modes for the two datasets based on the number of LOS satellites, DOP values, and RMS, with appropriate rankings assigned to each. Although none of the single-frequency modes were able to achieve successful positioning in the second dataset, the GPS system demonstrated the best performance in the different scenarios examined. In the dual integration mode, the combination of GPS and GLONASS yielded the best results, although the integration of GPS and Galileo also provided very similar outcomes. In the triple integration mode, the combination of GPS, GLONASS, and Galileo exhibited the best performance in positioning, while the combination of GPS, GLONASS, and BeiDou performed better in the first dataset. Finally, the four-system integration achieved the best performance in terms of accuracy and reliability among all modes. However, it is important to consider the associated limitations, including higher computational load, the need for more complex and capable hardware, greater signal bandwidth, and independent acquisition processes for each GNSS constellation. These factors collectively impose a trade-off that must be balanced against the performance gains achieved by multi-constellation integration. Furthermore, the choice of integrated systems should also take into account the specific application requirements.

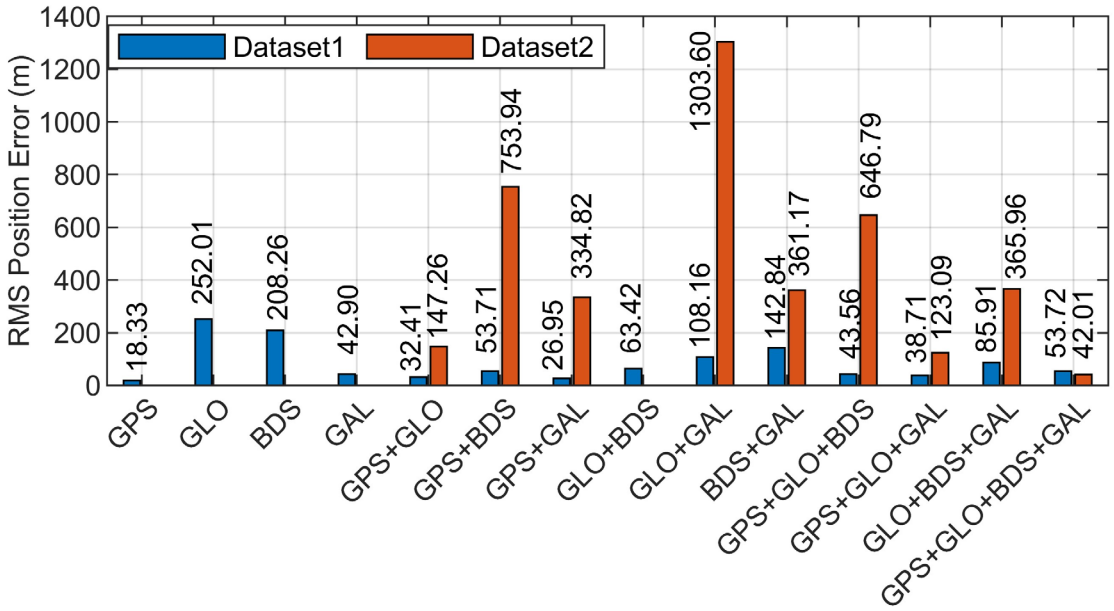

Fig 10. RMS results in different modes for the two datasets.

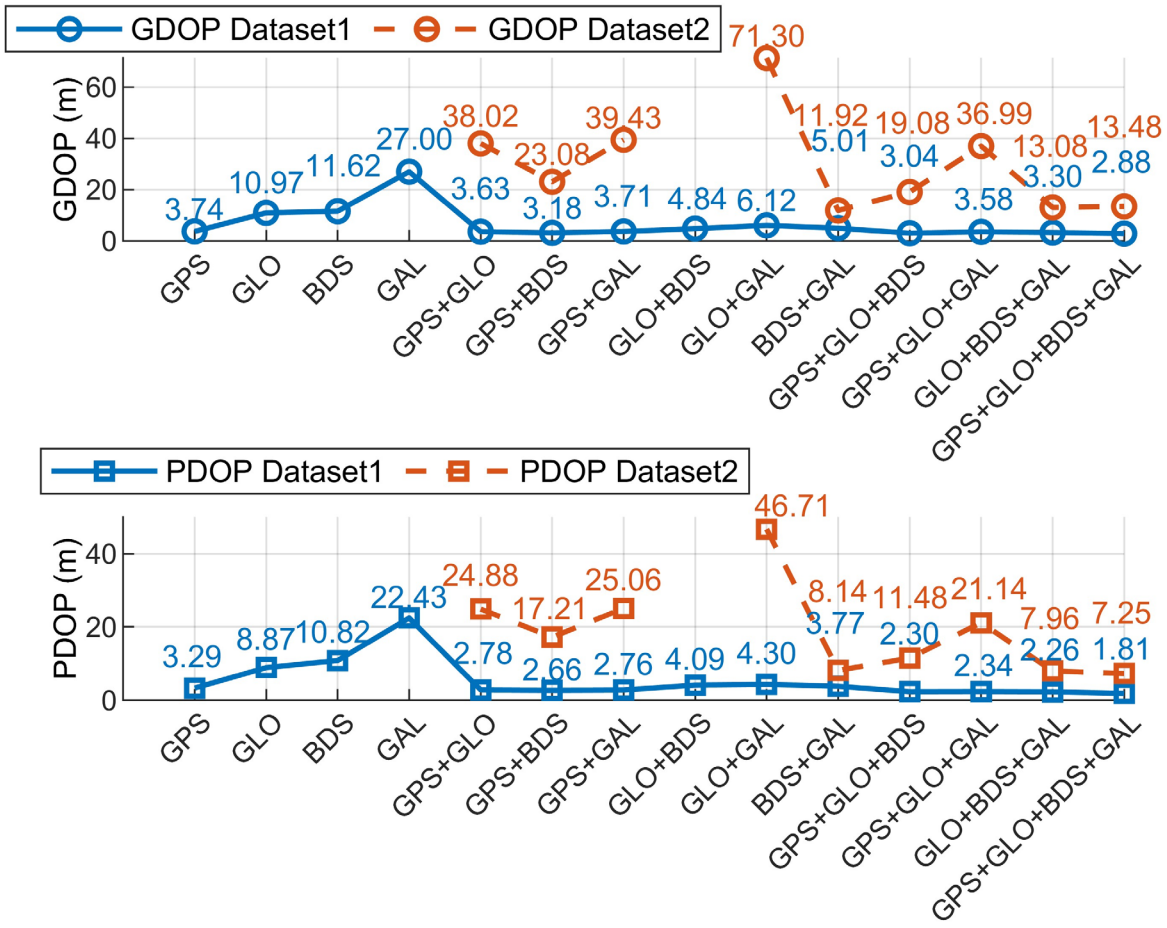

Fig 11. GDOP and PDOP results in different modes for the first and second datasets.

Table 4. Ranking of different modes based on the number of LOS satellites, DOP, and RMS.

Mode	Rank								Total
	Dataset 1			Total 1	Dataset 2			Total 2	
	RMS	DOP	No.		RMS	DOP	No.		
GPS	14	7	5	**26**	1	1	3	**5**	**31**
GLO	1	3	4	8	1	1	2	4	12
BDS	2	2	4	8	1	1	2	4	12
GAL	10	1	4	15	1	1	3	**5**	20
GPS+GLO	12	9	9	**30**	12	8	5	**25**	**55**
GPS+BDS	8	12	9	29	7	10	5	22	51
GPS+GAL	13	8	9	**30**	11	7	6	24	54
GLO+BDS	6	6	8	20	1	1	4	6	26
GLO+GAL	4	4	8	16	6	6	5	17	33
BDS+GAL	3	5	8	16	10	12	5	27	43
GPS+GLO+BDS	9	13	13	**35**	8	11	7	26	61
GPS+GLO+GAL	11	10	13	34	13	9	8	**30**	**64**
GLO+BDS+GAL	5	11	12	26	9	13	7	29	55
GPS+GLO+BDS+GAL	7	14	17	**38**	14	14	10	**38**	**76**

6 Conclusion

One effective method for mitigating the effects of blocking interference in GNSS systems is the integration of multiple different navigation systems during the positioning process. This approach reduces the likelihood of positioning loss due to physical obstructions by increasing the number of available satellites, allowing other systems to provide the necessary data and continue the positioning process. In this paper, the challenges related to system integration were examined, and innovative solutions in the navigation sector were presented. In various scenarios,

GNSS systems were integrated, and the results were analyzed from different perspectives. The findings indicated that system integration significantly enhances the reliability of the positioning process under blocking conditions. The choice of the appropriate integration method depends on various factors, including the intended application and the available hardware capabilities.

Conflict of Interest

The authors declare no conflict of interest.

Author Contributions

K. Bahmani: Conceptualization, Methodology, Software Development, Data Curation, Visualization, Investigation, and Writing – Original Draft. **A. Sadr:** Supervision, Investigation, and Writing – Review & Editing. **M. R. Mosavi:** Supervision, Investigation, and Writing – Review & Editing.

Funding

No funding was received for this work.

Informed Consent Statement

Not applicable.

References

[1] X. Chen, R. Luo, T. Liu, H. Yuan, and H. Wu, "Satellite navigation signal authentication in GNSS: a survey on technology evolution, status, and perspective for BDS," *Remote Sensing*, vol. 15, no. 5, pp. 1462, 2023.

[2] W. Liu, J. Liu, J. Xie, and B. Jiao, "Signal-in-space range error of the global BeiDou navigation satellite system and comparison with GPS, GLONASS, Galileo, and QZSS," *Journal of Surveying Engineering*, vol. 149, no. 1, pp. 04022013, 2023.

[3] Z. Li et al., "Assessment of the orbital variations of GNSS GEO and IGSO satellites for monitoring ionospheric TEC," *GPS Solutions*, vol. 27, no. 2, pp. 62, 2023.

[4] F. Menzione and M. Paonni, "LEO-PNT mega-constellations: a new design driver for the next generation MEO GNSS space service volume and spaceborne receivers," *IEEE/ION Position, Location and Navigation Symposium*, pp. 1196–1207, 2023.

[5] Z. Du, Q. Zhao, Y. Yao, and H. Zhu, "Real-time tropospheric delay map retrieval using sparse GNSS stations," *GPS Solutions*, vol. 28, no. 1, pp. 12, 2024.

[6] V. Hamza, B. Stopar, O. Sterle, and P. Pavlovčič-Prešeren, "Low-cost dual-frequency GNSS receivers and antennas for surveying in urban areas," *Sensors*, vol. 23, no. 5, pp. 2861, 2023.

[7] J. Cheng, C. Jiang, C. Jia, J. Ding, H. Li, and B. Qi, "Evaluation of Ionospheric Delay Extraction Model Using Dual-Frequency Multisystem Observations," *IEEE Sensors Journal*, vol. 23, no. 14, pp. 16197–16209, 2023.

[8] D. Weng, Z. Hou, Y. Meng, M. Cai, and Y. Chan, "Characterization and mitigation of urban GNSS multipath effects on smartphones," *Measurement*, vol. 223, pp. 113766, 2023.

[9] K. Bahmani, M. R. Mosavi, A. Sadr, and H. S. Shahhoseini, "Employing a two-stage process with resampling, decision rules, and fine acquisition to optimize the acquisition stage of GNSS receiver performance," *Scientific Reports*, vol. 14, no. 1, pp. 22463, 2024.

[10] P. Defraigne, E. Pinat, and B. Bertrand, "Impact of Galileo-to-GPS-Time-Offset accuracy on multi-GNSS positioning and timing," *GPS Solutions*, vol. 25, pp. 1–15, 2021.

[11] A. Kumari and D. Bhatt, "Advanced system analysis and survey on the GPS receiver front end," *IEEE Access*, vol. 10, pp. 24611–24626, 2022.

[12] K. Bahmani, M. Nezhadshahbodaghi, and M. R. Mosavi, "Optimisation of doppler search space to improve acquisition speed of GPS signals," *Survey Review*, vol. 55, no. 390, pp. 216–232, 2023.

[13] K. Borre, I. Fernández-Hernández, J. A. López-Salcedo, and M. Z. H. Bhuiyan, "GNSS Software Receivers," Cambridge University Press, 2022.

[14] K. Bahmani, M. Nezhadshahbodaghi, and M. R. Mosavi, "Reduction of the acquisition time in GPS receiver by multi-stage frequency bins," *10th International Symposium on Telecommunications (IST)*, pp. 170–174, 2020.

[15] W. Jianing, L. Baowang, and X. Zhe, "Weak GPS signal acquisition method based on DBZP," *Journal of systems engineering and electronics*, vol. 29, no. 2, pp. 236–243, 2018.

[16] M. Sharie, M. R. Mosavi, and N. Rahemi, "Acquisition of weak GPS signals using wavelet-based de-noising methods," *Survey Review*, vol. 52, no. 375, pp. 497–513, 2020.

[17] X. Ding, Y. Yang, and J. Chen, "Improved high-sensitivity partial-matched filter with FFT-based

acquisition algorithm for BDS-2 and BDS-3 signals with secondary code modulation," *GPS Solutions*, vol. 27, no. 3, pp. 143, 2023.

[18] K. Sun, M. Elhajj, and W. Y. Ochieng, "A GNSS Anti-Interference Method based on Fractional Fourier Transform," *IEEE Transactions on Aerospace and Electronic Systems*, 2024.

[19] S. H. Kong, "High sensitivity and fast acquisition signal processing techniques for GNSS receivers: From fundamentals to state-of-the-art GNSS acquisition technologies," *IEEE Signal Processing Magazine*, vol. 34, no. 5, pp. 59–71, 2017.

[20] Q. Liu, Y. Kou, Z. Huang, J. Wang, and Y. Yao, "Mean acquisition time analysis for GNSS parallel and hybrid search strategies," *GPS Solutions*, vol. 23, pp. 1–13, 2019.

[21] F. Hao, B. Yu, X. Gan, R. Jia, H. Zhang, L. Huang, and B. Wang, "Unambiguous acquisition/tracking technique based on sub-correlation functions for GNSS sine-BOC signals," *Sensors*, vol. 20, no. 2, pp. 485, 2020.

[22] Y. Cheng and Q. Chang, "A carrier tracking loop using adaptive strong tracking Kalman filter in GNSS receivers," *IEEE Communications Letters*, vol. 24, no. 12, pp. 2903–2907, 2020.

[23] I. P. Portella, A. de O. Moraes, M. da Silva Pinho, J. Sousasantos, and F. Rodrigues, "Examining the tolerance of GNSS receiver phase tracking loop under the effects of severe ionospheric scintillation conditions based on its bandwidth," *Radio Science*, vol. 56, no. 6, pp. 1–11, 2021.

[24] T. Zhang, J. Shi, T. Lin, X. Feng, and X. Niu, "GNSS position-aided delay-locked loops for accurate urban navigation," *GPS Solutions*, vol. 27, no. 3, pp. 127, 2023.

[25] R. Yang, Y. Morton, K. V. Ling, and E. K. Poh, "Generalized GNSS signal carrier tracking—Part II: Optimization and implementation," *IEEE Transactions on Aerospace and Electronic Systems*, vol. 53, no. 4, pp. 1798–1811, 2017.

[26] D. J. Jwo, Z. M. Wen, and Y. C. Lee, "Vector tracking loop assisted by the neural network for GPS signal blockage," *Applied Mathematical Modelling*, vol. 39, no. 19, pp. 5949–5968, 2015.

[27] R. Yang, J. Huang, X. Zhan, and S. Luo, "Decentralized FLL-assisted PLL design for robust GNSS carrier tracking," *IEEE Communications Letters*, vol. 25, no. 10, pp. 3379–3383, 2021.

[28] A. Hussain, A. Ahmed, H. Magsi, and R. Tiwari, "Adaptive GNSS receiver design for highly dynamic multipath environments," *IEEE Access*, vol. 8, pp. 172481–172497, 2020.

[29] P. Steigenberger, O. Montenbruck, M. Bradke, M. Ramatschi, and U. Hessels, "Evaluation of earth rotation parameters from modernized GNSS navigation messages," *GPS Solutions*, vol. 26, no. 2, pp. 50, 2022.

[30] K. Zhang, E. G. Larsson, and P. Papadimitratos, "Protecting GNSS open service navigation message authentication against distance-decreasing attacks," *IEEE Transactions on Aerospace and Electronic Systems*, vol. 58, no. 2, pp. 1224–1240, 2021.

[31] S. Söderholm, M. Z. H. Bhuiyan, S. Thombre, L. Ruotsalainen, and H. Kuusniemi, "A multi-GNSS software-defined receiver: Design, implementation, and performance benefits," *Annals of Telecommunications*, vol. 71, no. 7, pp. 399–410, 2016.

[32] M. Lu, W. Li, Z. Yao, and X. Cui, "Overview of BDS III new signals," *Navigation*, vol. 66, no. 1, pp. 19–35, 2019.

[33] L. Ortega, C. Poulliat, M. L. Boucheret, M. Aubault-Roudier, and H. Al-Bitar, "Optimizing the co-design of message structure and channel coding to reduce the TTD for a Galileo 2nd generation signal," *Navigation*, vol. 67, no. 3, pp. 471–492, 2020.

[34] D. L. Warren and J. F. Raquet, "Broadcast vs. precise GPS ephemerides: A historical perspective," *GPS Solutions*, vol. 7, pp. 151–156, 2003.

[35] P. Zabalegui, G. De Miguel, A. Perez, J. Mendizabal, J. Goya, and I. Adin, "A review of the evolution of the integrity methods applied in GNSS," *IEEE Access*, vol. 8, pp. 45813–45824, 2020.

[36] X. Zuo, J. Bu, X. Li, J. Chang, and X. Li, "The quality analysis of GNSS satellite positioning data," *Cluster computing*, vol. 22, pp. 6693–6708, 2019.

[37] F. Rahman, E. Aghapour, and J. A. Farrell, "Vehicle ECEF position accuracy and reliability in the presence of DGNSS communication latency," *IEEE Intelligent Transportation Systems Magazine*, vol. 13, no. 4, pp. 262–272, 2020.

[38] R. Xu, M. Ding, Y. Qi, S. Yue, and J. Liu,

"Performance analysis of GNSS/INS loosely coupled integration systems under spoofing attacks," *Sensors*, vol. 18, no. 12, pp. 4108, 2018.

[39] V. K. D. Srinivasu, N. Dashora, D. S. V. V. D. Prasad, and K. Niranjan, "Loss of lock on GNSS signals and its association with ionospheric irregularities observed over Indian low latitudes," *GPS Solutions*, vol. 26, no. 1, pp. 34, 2022.

[40] Y. Lee and B. Park, "Nonlinear regression-based GNSS multipath modelling in deep urban area," *Mathematics*, vol. 10, no. 3, pp. 412, 2022.

[41] X. Zhang, F. Zhu, X. Tao, and R. Duan, "New optimal smoothing scheme for improving relative and absolute accuracy of tightly coupled GNSS/SINS integration," *GPS Solutions*, vol. 21, pp. 861–872, 2017.

[42] T. Li, H. Zhang, X. Niu, and Z. Gao, "Tightly-coupled integration of multi-GNSS single-frequency RTK and MEMS-IMU for enhanced positioning performance," *Sensors*, vol. 17, no. 11, pp. 2462, 2017.

[43] D. Weng, W. Chen, Y. Lu, S. Ji, H. Luo, and M. Cai, "Global DGNSS service for mobile positioning through public corrections," *Advances in Space Research*, vol. 72, no. 10, pp. 4402–4412, 2023.

[44] D. Weng, S. Ji, Y. Lu, W. Chen, and Z. Li, "Improving DGNSS performance through the use of network RTK corrections," *Remote Sensing*, vol. 13, no. 9, pp. 1621, 2021.

[45] T. Dautermann, T. Ludwig, R. Geister, and L. Ehmke, "Extending access to localizer performance with vertical guidance approaches by means of an SBAS to GBAS converter," *GPS Solutions*, vol. 24, pp. 1–13, 2020.

[46] N. Sokolova, A. Morrison, and A. Diez, "Characterization of the GNSS RFI threat to DFMC GBAS signal bands," *Sensors*, vol. 22, no. 22, pp. 8587, 2022.

[47] C. Cai, Y. Gao, L. Pan, and J. Zhu, "Precise point positioning with quad-constellations: GPS, BeiDou, GLONASS and Galileo," *Advances in* Space Research, vol. 56, no. 1, pp. 133–143, 2015.

[48] W. Li, Q. Yang, X. Du, M. Li, Q. Zhao, L. Yang, and G. Qin, "LEO augmented precise point positioning using real observations from two CENTISPACE™ experimental satellites," *GPS Solutions*, vol.28, no1, pp.44, 2024.

[49] J. Chen, X. Zhao, C. Liu, S. Zhu, Z. Liu, and D. Yue, "Evaluating the latest performance of precise point positioning in multi-GNSS/RNSS: GPS, GLONASS, BDS, Galileo and QZSS," *The Journal of Navigation*, vol. 74, no. 1, pp. 247–267, 2021.

[50] H. Ma, Q. Zhao, S. Verhagen, D. Psychas, and X. Liu, "Assessing the performance of multi-GNSS PPP-RTK in the local area," *Remote Sensing*, vol. 12, no. 20, pp. 3343, 2020.

[51] N. Kubo, K. Kobayashi, and R. Furukawa, "GNSS multipath detection using continuous time-series C/N0," Sensors, vol. 20, no. 14, pp. 4059, 2020.

[52] T. Suzuki, "Multiple update particle filter: position estimation by combining GNSS pseudo-range and carrier phase observations," *IEEE International Conference on Robotics and Automation*, pp. 13680-13686, 2024.

[53] Z. Pan, H. Chai, and Y. Kong, "Integrating multi-GNSS to improve the performance of precise point positioning," *Advances in Space Research*, vol. 60, no. 12, pp. 2596–2606, 2017.

[54] X. Weng, K. Ling, H. Liu, and K. Cao, "Towards end-to-end GPS localization with neural pseudorange correction," *27th IEEE International Conference on Information Fusion*, pp. 1-7, 2024.

[55] K. Wang, P. J. Teunissen, and A. El-Mowafy, "The ADOP and PDOP: Two complementary diagnostics for GNSS positioning," *Journal of Surveying Engineering*, vol. 146, no. 2, pp. 04020008, 2020.

[56] R. Dach, S. Schaer, S. Lutz, M. Meindl, and G. Beutler, "Combining the observations from different GNSS," In EUREF 2010 Symposium, pp. 2–5, 2010.

[57] R. Wang G. Marut, T. Hadaś, and T. Hobiger, "Improving GNSS meteorology by fusing measurements of several colocated receivers on the observation level," *IEEE Journal of Selected Topics in Applied Earth Observations and Remote Sensing*, vol. 17, pp. 7841-7851, 2024.

Biographies

K. Bahmani holds a B.S. in Electronic Engineering from the University of Kurdistan, which he earned in 2017, and an M.S. in the same field from the Iran University of Science and Technology (IUST), completed in 2021. Currently, he is a Ph.D. student at the Department of Electrical Engineering, IUST, with research interests spanning signal processing, GNSS applications, 3-D FPGAs, and artificial intelligence.

A. Sadr received the Ph.D. degree in Instrumentation from Department of instrumentation & Analytical Science (DIAS), University of Manchester Institute of Science and Technology (UMIST), Manchester, England in 2002. He is currently an Associate Professor in Electronic Engineering Department of Iran University of Science and Technology (IUST). His research interest includes nondestructive evaluation, medical instrumentation, and microprocessor & microcontroller- based systems design.

M. R. Mosavi received his B.Sc., M.Sc., and Ph.D. degrees in Electronic Engineering from Iran University of Science and Technology (IUST), Tehran, Iran in 1997, 1998, and 2004, respectively. He is currently a faculty member (Full Professor) of the Department of Electrical Engineering of IUST. He is the author of more than 600 scientific publications in journals and international conferences in addition to 15 academic books. His research interests include circuits and systems design. He is also editor in-chief of “Iranian Journal of Marine Technology” and editorial board member of “Iranian Journal of Electrical and Electronic Engineering” and “GPS Solutions”.